SRI International

AFOSR-TR- [illegible] 4

Annual Report No. 1 • October 1993

MICROSTRUCTURE/PROPERTY RELATIONSHIPS FOR SCS6/TIMETAL 21-S COMPOSITE

Charles G. Schmidt, Senior Materials Scientist
Takao Kobayashi, Senior Research Engineer
Christine H. Kanazawa, Materials Scientist
Donald A. Shockey, Associate Director
Poulter Laboratory

Prepared for:

Air Force Office of Scientific Research
AFOSR/NA
Directorate of Aerospace Sciences
Building 410
Bolling AFB, DC 20332-6448

Attn: Dr. Walter Jones

Approved:

James D. Colton, Director
Poulter Laboratory

David M. Golden
Vice President
Physical Sciences Division

333 Ravenswood Avenue • Menlo Park, CA 94025-3493 • (415) 326-6200 • FAX: (415) 326-5512 • Telex 334486

REPORT DOCUMENTATION PAGE

Form Approved OMB No. 0704-0188

1. AGENCY USE ONLY *(Leave blank)*	2. REPORT DATE	3. REPORT TYPE AND DATES COVERED
	October 1993	Annual Report 010992 - 310893

4. TITLE AND SUBTITLE

Microstructure/Property Relationships for SCS6/Timetal 21-S Composite (w)

5. FUNDING NUMBERS

F49620-92-C-0063

FQ8671-9201544 2302/BS

6. AUTHOR(S)

Charles G. Schmidt, Takao Kobayashi, Christine H. Kanazawa, and Donald A. Shockey

7. PERFORMING ORGANIZATION NAME(S) AND ADDRESS(ES)

SRI International
333 Ravenswood Avenue
Menlo Park, CA 94025-3493

8. PERFORMING ORGANIZATION REPORT NUMBER

PYU-3894

9. SPONSORING/MONITORING AGENCY NAME(S) AND ADDRESS(ES)

Air Force Office of Scientific Research
Building 410
Bolling AFB, DC 20332-6448

NA

10. SPONSORING/MONITORING AGENCY REPORT NUMBER

11. SUPPLEMENTARY NOTES

12a. DISTRIBUTION/AVAILABILITY STATEMENT

UNCLASSIFIED/UNLIMITED

12b. DISTRIBUTION CODE

13. ABSTRACT *(Maximum 200 words)*

Fracture surfaces of tensile test specimens from SCS6/Timetal 21-S composites with $[0]_4$ or $[0/90]_s$ ply sequences were examined to characterize the failure processes. Fracture surface topography analysis (FRASTA) was used to quantitatively characterize the fracture surfaces. Results indicate that the topographies of the matrix fracture surfaces are a strong function of processes that occur during the rapid reduction in load after the maximum load. Failure of the matrix in all composites occurs after the maximum load is reached and after some or all of the 0° fibers have failed. Only part of the matrix phase of the 90° plies in a $[0/90]_s$ composite contributes to the tensile strength. The interface strength between the fibers and the matrix is negligible and does not contribute significantly to the strength of the composite.

14. SUBJECT TERMS			15. NUMBER OF PAGES
Metal Matrix Composites	Tensile Test	SiC Fiber	21
Mechanical Properties	Fracture Surface Analysis	Titanium Alloy	16. PRICE CODE

17. SECURITY CLASSIFICATION OF REPORT	18. SECURITY CLASSIFICATION OF THIS PAGE	19. SECURITY CLASSIFICATION OF ABSTRACT	20. LIMITATION OF ABSTRACT
UNCLASSIFIED	UNCLASSIFIED	UNCLASSIFIED	UL

CLASSIFIED BY:

N/A since Unclassified.

DECLASSIFY ON:

N/A since Unclassified.

INTRODUCTION

A critical need exists for structural materials that have high specific strength and stiffness and good oxidation resistance and can be used in advanced aerospace applications. A family of materials that promises to answer many of these needs is titanium metal matrix composites. One of the challenges to be overcome, however, is to tailor the properties of metal matrix composites to match the specific requirements for a given application. To do so requires a clear and accurate understanding of the deformation and failure behavior of the composites and the underlying mechanisms that affect them.

The present study is designed to assist in developing this understanding through a more careful and more quantitative examination of fracture surfaces produced in mechanical tests of the SCS6/Timetal 21-S composite. The discussion that follows outlines the results from an analysis of several tensile tests and identifies the direction of future research.

RESULTS

Tensile specimens of SCS6/Timetal 21-S composite were provided by The University of Dayton Research Institute (UDRI) for fracture surface analysis and model development. Tensile specimens with composite lay-ups of $[0]_4$, $[0/90]_S$, and $[0/\pm45/90]_S$ that were tested at 23°, 500°, 650°, and 815°C were received with stress-strain curves obtained by UDRI. Table 1 summarizes the test conditions and tensile results for the specimens received. This table includes all specimens tested by UDRI that were provided for this investigation.

Fracture Surface Examination

Figures 1 and 2 show scanning electron microscope (SEM) micrographs of fracture surfaces from $[0]_4$ tensile specimens tested at 23° and 815°C, respectively. The fracture surface of the matrix component of the specimen tested at 23°C (Figure 2) exhibits the features of a material that failed in a ductile manner; however, in one of the composite plies, remnants of a woof fiber is clearly evident (see Figure 1e). Evidence of the fiber appears on both sides of the fracture surface. An X-ray energy dispersive spectrometer (EDS) analysis of the woof fiber indicated that its composition is high in molybdenum (see Table 2). The measured compositions of the matrix and the fiber are consistent with the nominal compositions of Timetal 21-S and SiC, respectively.

Table 1

SCS6/TIMETAL 21-S COMPOSITE TENSILE TEST DATA

Specimen Designation	Lay-up	Area mm^2	Test Temperature °C	Room Temperature Modulus GPa	Test Temperature Modulus GPa	Yield Strength MPa	Maximum Tensile Strength MPa	Elongation to Failure %	Fracture Surface Available for Analysis
91-253	$[0]_4$	4.6626	23	209.6	209.6	1307	2005	1.7	no
91-254	$[0]_4$	4.7782	23	197.1	197.1	1853	1983	1.4	yes
91-250	$[0]_4$	6.0632	500	222.2	189.7	not available	1487	0.94	yes
91-251	$[0]_4$	6.0393	500	215.3	194.1	not available	1449	0.88	yes
91-249	$[0]_4$	6.0871	500	214.6	187.9	not available	1399	0.88	yes
91-252	$[0]_4$	6.0632	650	231.6	175.7	1141	1141	0.86	yes
91-248	$[0]_4$	6.0632	650	194.0	185.7	1083	1203	0.94	yes
91-247	$[0]_4$	6.0632	815	not available	135.0	not available	936	0.79	yes
91-220	$[0/90]_s$	4.7264	23	154.2	154.2	882.4	1135.7	1.14	yes
91-219	$[0/90]_s$	9.4768	23	156.1	156.1	911.8	1042.6	0.96	no
91-216	$[0/90]_s$	6.0393	500	178.4	120.0	865.5	882.7	0.94	yes
91-215	$[0/90]_s$	11.9832	500	187.1	120.4	864.3	885.7	0.93	yes
91-217	$[0/90]_s$	6.0393	650	164.3	106.9	623.9	644.1	0.85	no
91-214	$[0/90]_s$	12.0071	650	165.5	136.7	495.9	630.6	0.89	yes
91-218	$[0/90]_s$	6.2516	815	not available	124.8	394.0	495.0	0.75	no
91-213	$[0/90]_s$	11.9593	815	not available	116.2	334.5	480.0	0.97	yes
91-288	$[0/\pm45/90]_s$	9.2129	23	141.8	141.8	593.9	783.5	0.97	yes
91-287	$[0/\pm45/90]_s$	18.0645	23	156.4	156.4	not available	did not fail	did not fail	no
91-284	$[0/\pm45/90]_s$	11.4406	500	155.0	120.0	575.9	598.3	0.74	yes
91-283	$[0/\pm45/90]_s$	22.4806	500	165.2	124.9	592.2	645.9	0.79	yes
91-286	$[0/\pm45/90]_s$	11.6516	650	158.2	121.8	329.1	436.6	0.76	yes
91-282	$[0/\pm45/90]_s$	22.8516	650	162.4	128.4	335.6	466.0	0.88	no
91-281	$[0/\pm45/90]_s$	22.5251	650	160.2	111.6	367.9	436.2	not available	no
91-285	$[0/\pm45/90]_s$	11.8180	815	not available	110.6	207.2	314.7	0.73	no

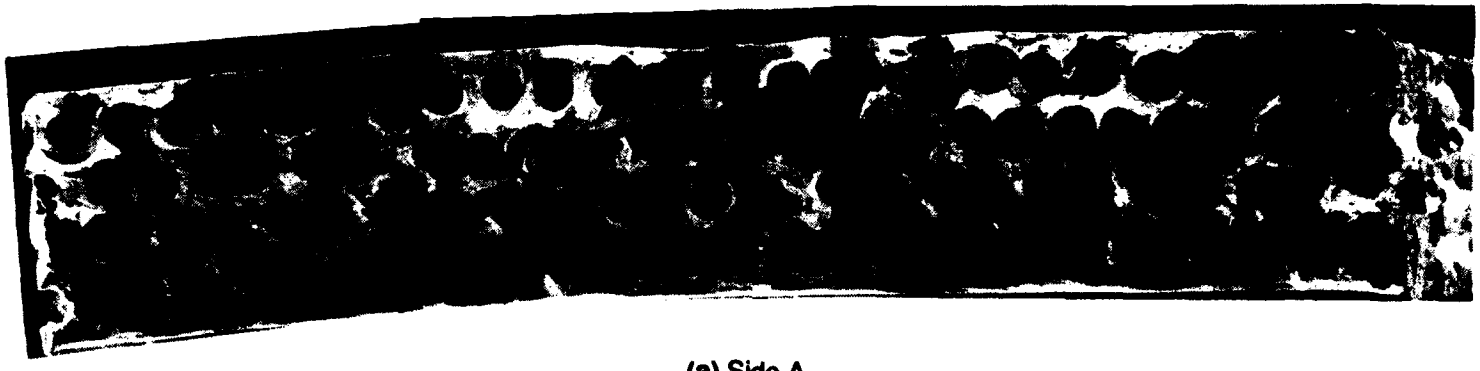

(a) Side A

(b) Side B

100 µm

CPM-3894-1

Figure 1. SEM micrographs of the fracture surfaces from the 23°C tensile test of Specimen 91-254.

(c) Orthogonal high magnification view of area on Side A

(d) Angled high magnification view of area on Side A

50 µm

CPM-3894-2

Figure 1. SEM micrographs of the fracture surfaces from the 23°C tensile test of Specimen 91-254. (Continued)

(e) High magnification view showing molybdenum fiber

100 μm

CPM-3894-3

Figure 1. SEM micrographs of the fracture surfaces from the 23°C tensile test of Specimen 91-254. (Concluded)

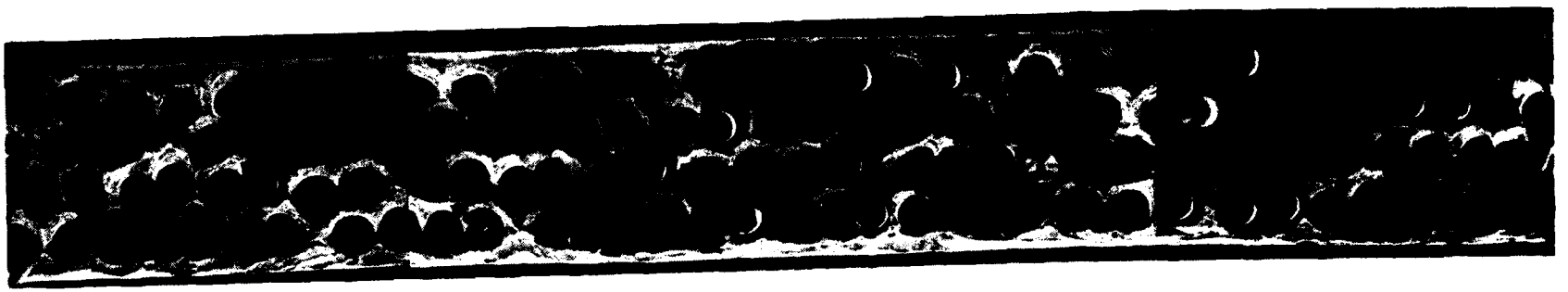

(a) Side A

(b) Side B

100 µm

CPM-3894-4

Figure 2. SEM micrographs of the fracture surfaces resulting from the 815°C tensile test of Specimen 91-247.

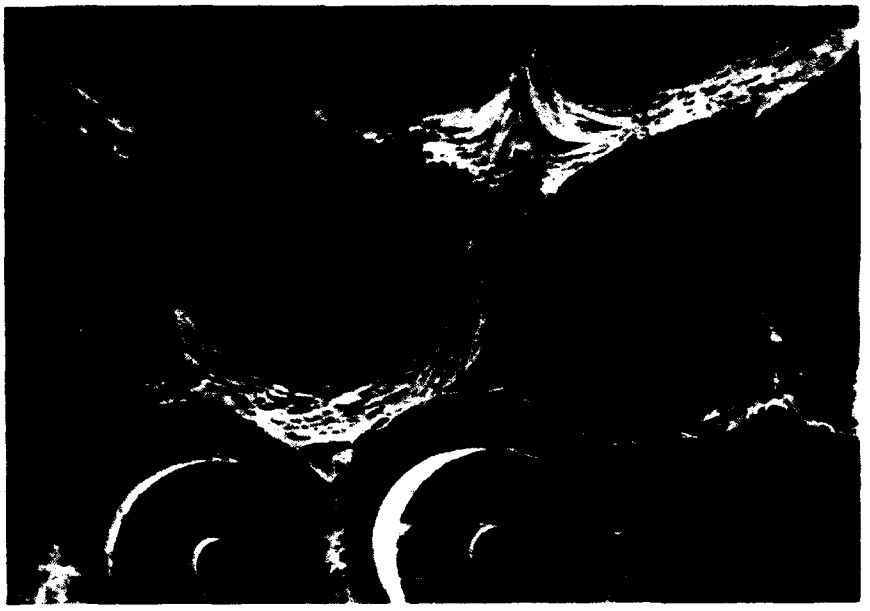

(c) Orthogonal high magnification view of area on Side A

(d) Angled high magnification view of area on Side A

50 μm

CPM-3894-5

Figure 2. SEM micrographs of the fracture surfaces resulting from the 815°C tensile test of Specimen 91-247. (Concluded)

Table 2

TYPICAL COMPOSITIONS OF THE WOOF FIBER, MATRIX, AND SIC FIBER ON THE FRACTURE SURFACE OF SPECIMEN 91-254

	Composition (weight percent)			
Location	Ti	Si	Mo	Al
Woof Fiber	15.0	1.9	82.4	0.8
Matrix	84.1	1.7	13.6	0.6
SiC Fiber	0.6	92.4	5.3	1.6

The appearance of the matrix material on the fracture surface of the $[0]_4$ tensile specimen tested at 815°C shows greater ductility than the fracture surfaces from the 23°C test. To better compare the differences between the specimens tested at these two temperatures, a scanning laser microscope was used to topographically characterize representative regions of the fracture surfaces from tensile specimens tested at 23° and 815°C, as shown in Figure 3. Figure 4 compares the fracture surface profile of the matrix material between two fibers in 23° and 815°C test specimens. The fracture surfaces of the matrix from the 23°C test are relatively flat and at an angle that suggests a ductile shear dominated failure process. The fracture surface of the matrix material in the 815°C test indicates a ductile necking type of failure.

Stress-Strain Behavior Examination

An analysis of the stress-strain behavior was undertaken to assist in determining the significance of the fractographic features. Through the analysis described below, we came to the conclusion that the fracture surface features strongly reflect the matrix deformation which occurs after the maximum stress is reached. The magnitude of the maximum stress is primarily determined by the fiber strength and the nonelastic deformation of the matrix.

Figure 5 compares the stress-strain responses of several $[0]_4$ and $[0/90]_S$ tensile test specimens that were examined in this investigation. To estimate the contribution of the matrix and the fibers to the stress-strain behavior of the tests on $[0]_4$ composite shown in Figure 5a, an isostrain rule-of-mixtures (ROM) approach was employed, with no bonding between the fibers and the matrix. This approach is consistent with that used by Larsen and Nicholas[1] and by Neu and Nicholas[2] in their analysis of thermomechanical fatigue of SCS6/Timetal 21-S composites. We assumed that no damage (i.e., cracking) occurs to the matrix during loading until the maximum load is reached. The stress-strain behavior of the Timetal 21-S matrix material was determined from a version of the Bodner-Partom model developed by Neu.[3] Figure 6 shows calculations of the fraction of the load borne by the fibers in $[0]_4$ composite tensile tests at various temperatures.

---

[1] J. M. Larsen and T. Nicholas, "Mechanical Behavior and Damage Tolerance and Titanium Matrix Composites," overview presentation of work performed by Wright Laboratory Materials Directorate in Government Work Package (GWP) 85.

[2] R. W. Neu and T. Nicholas, "Effect of Laminate Orientation on the Thermomechanical Fatigue Behavior of a Titanium Matrix Composite," submitted to the Journal of Composites Technology and Research.

[3] R. W. Neu, "Nonisothermal Material Parameters for the Bodner-Partom Model," paper presented at the Symposium on Parameter Estimation for Modern Constitutive Equations, ASME Winter Annual Meeting, Nov. 28 - Dec. 3, 1993, New Orleans, LA.

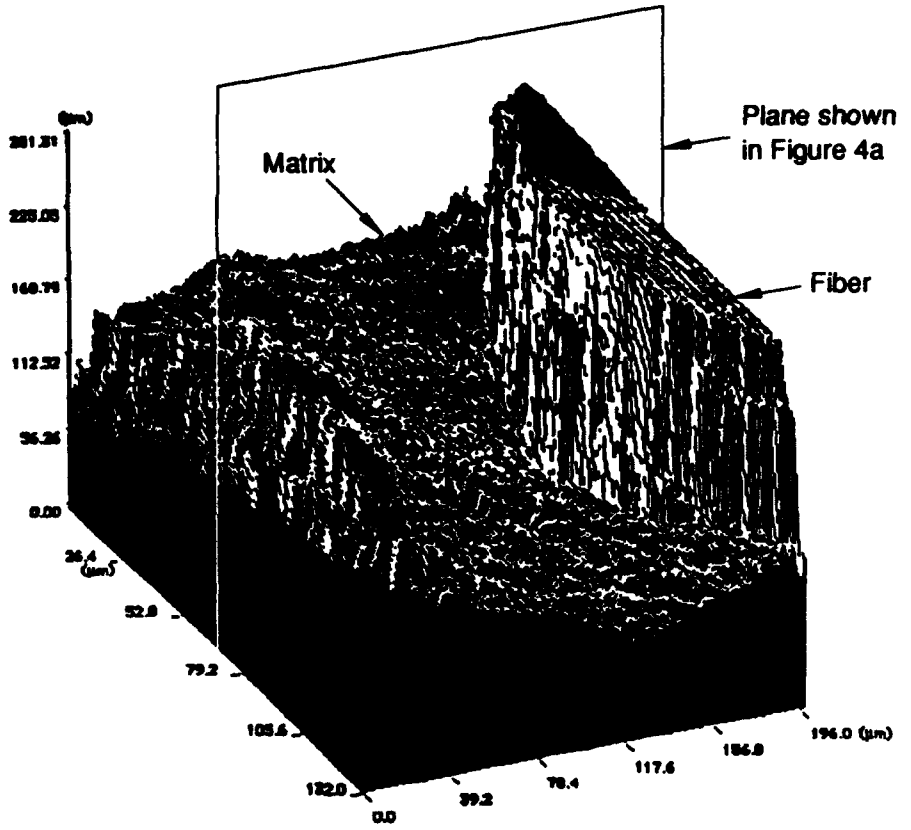

(a) Top fracture surface profile in Figure 4a (23°C test; Specimen 91-254)

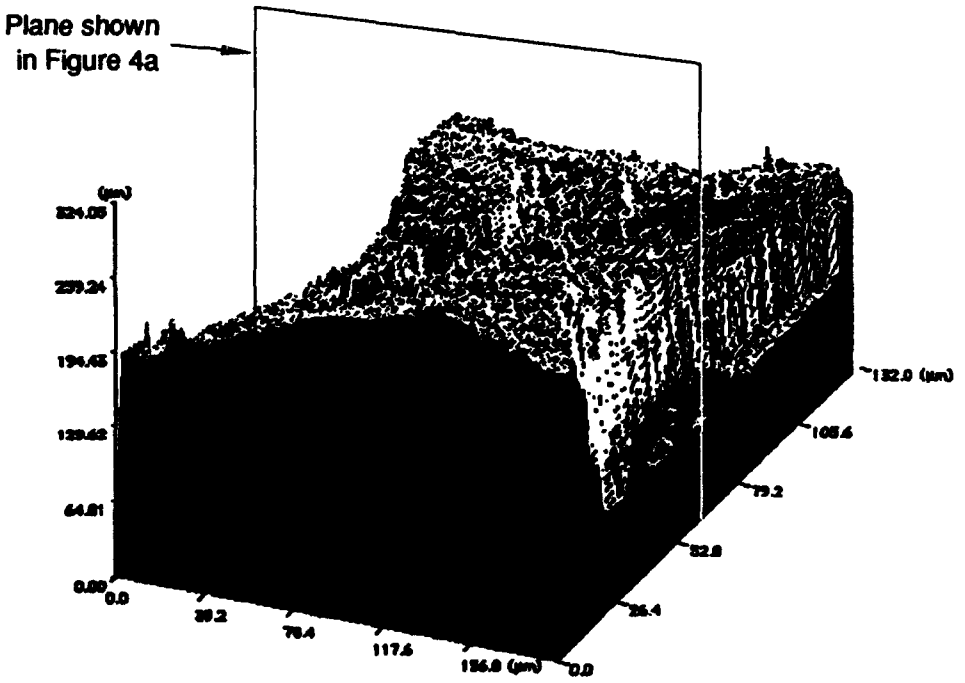

(b) Bottom fracture surface profile in Figure 4a (23°C test; Specimen 91-254)

CM-3894-6

Figure 3. Fracture surface profiles measured with a scanning laser microscope.

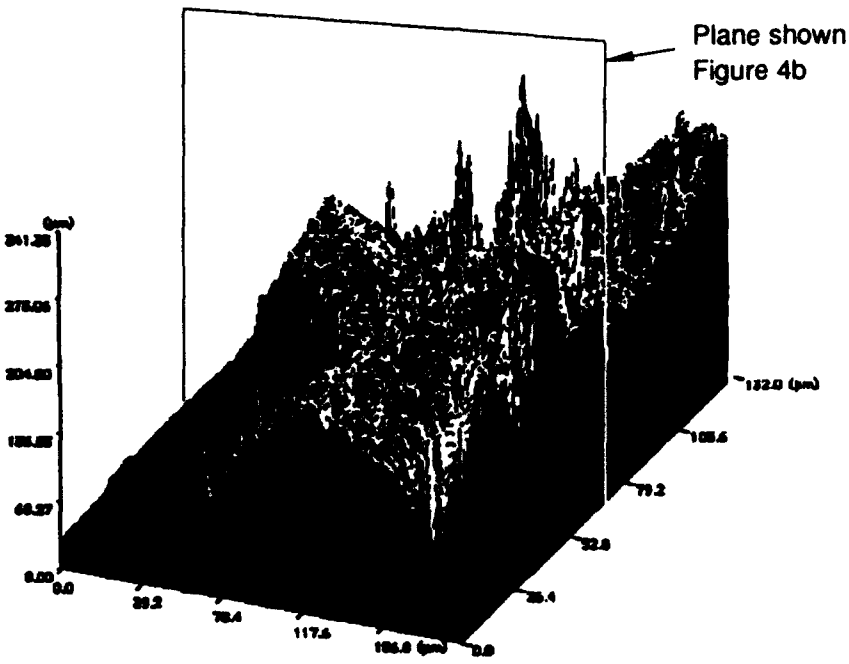

(c) Top fracture profile in Figure 4b (815°C test; Specimen 91-247)

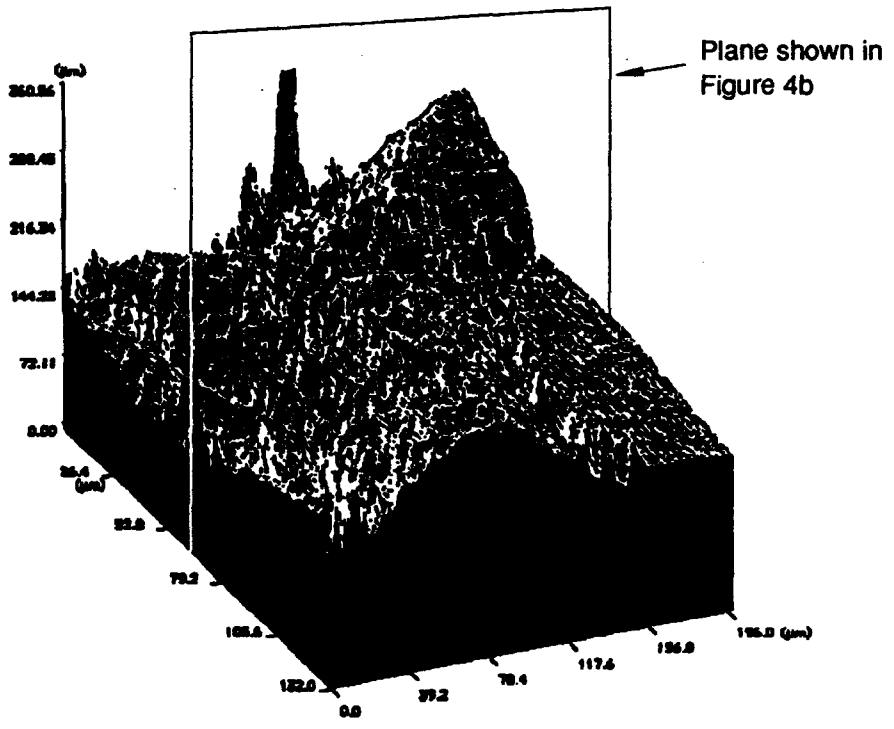

(d) Bottom fracture surface profile in Figure 4b (815°C test; Specimen 91-247)

CM-3894-7

Figure 3. Fracture surface profiles measured with a scanning laser microscope. (Concluded)

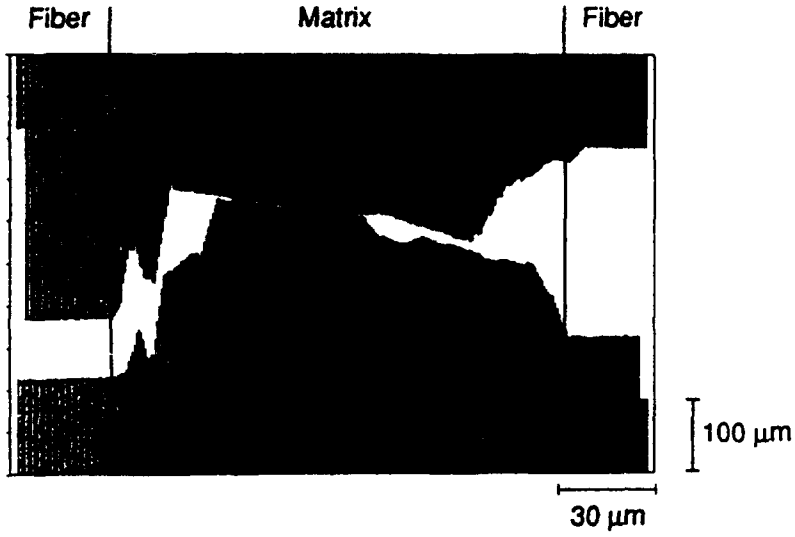

(a) 23°C Test; Specimen 91-2154

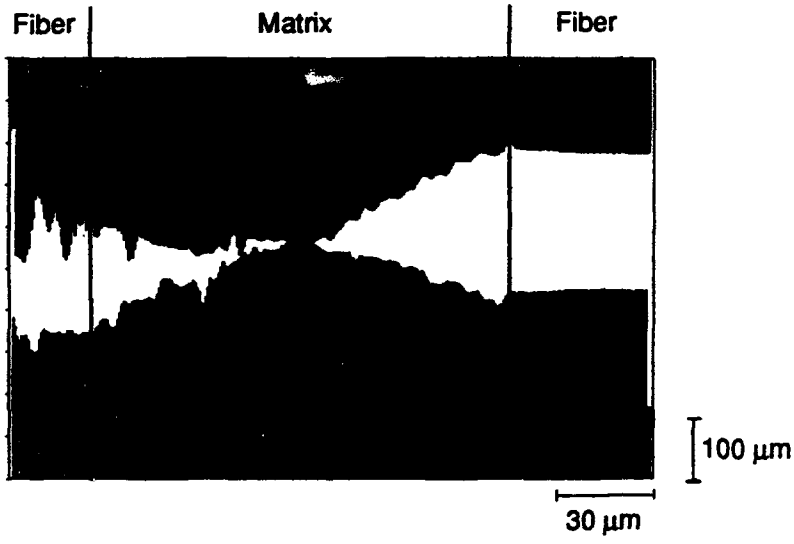

(b) 815°C Test; Specimen 91-247

CA-3894-8

Figure 4. Conjugate fracture surface profile from $[0]_4$ tensile test specimens.

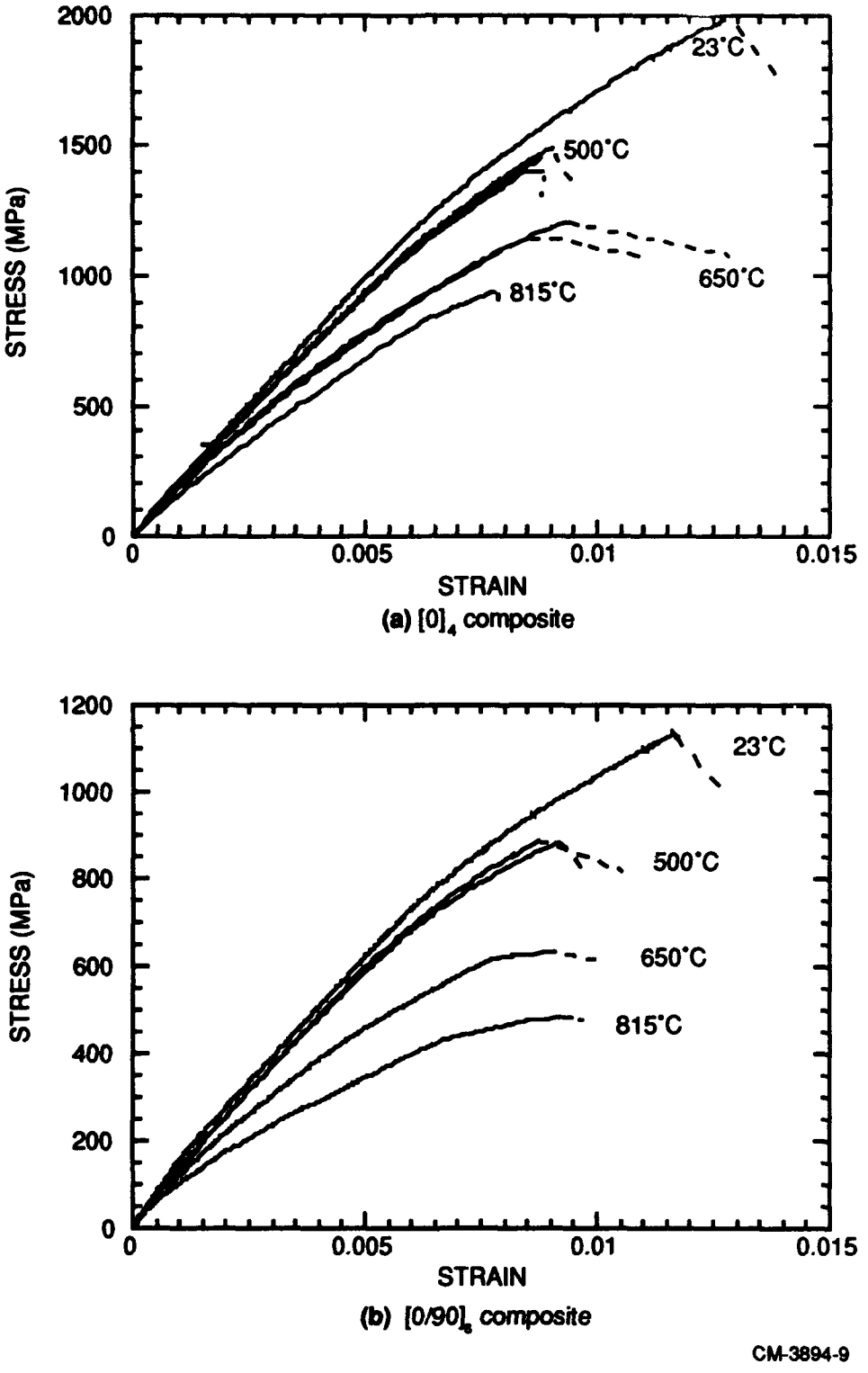

Figure 5. Stress-strain curves for SCS6/Timetal 21-S composite.

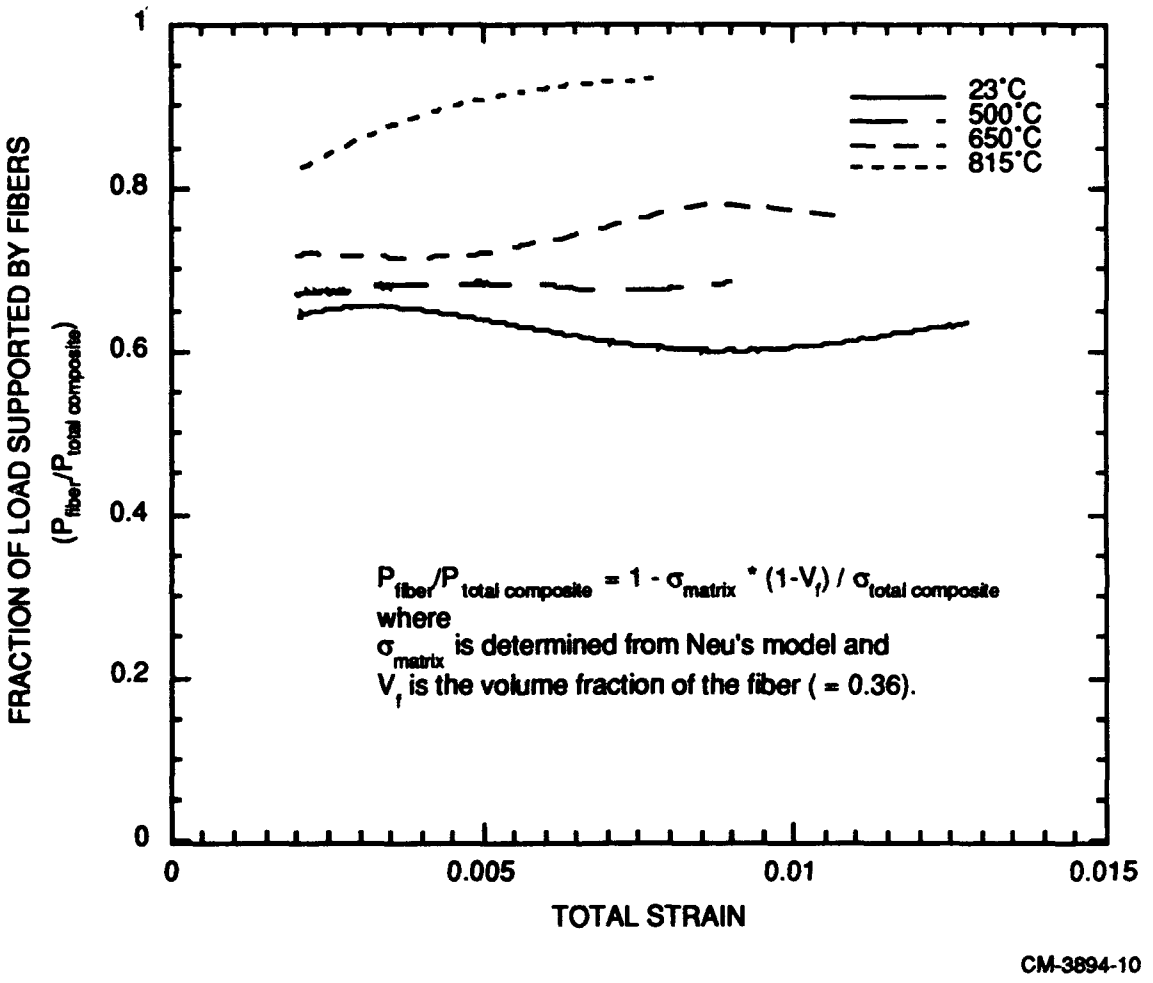

Figure 6. Fraction of the load supported by fibers in tensile tests on $[0]_4$ SCS6/Timetal 21-S composite.

These ratios were determined by subtracting the matrix contribution obtained from Neu's model from the measured stress-strain behavior of the composite and dividing this difference by the measured stress-strain behavior of the composite. Figure 6 shows that the fibers bear a majority of the load in all cases (i.e., a little more than 60% of the load at 23°C and as much as 93% of the load at 815°C).

A prediction of the stress-strain response of the $[0/90]_s$ composite was produced that was based on the following assumptions:

- The bond strength between the fiber and the matrix is negligible.
- The matrix is not damaged (i.e., does not crack) until after the maximum load is reached.
- The isostrain ROM model is valid for the conditions examined.
- The contribution of the 90° plies to the strength of the composite is from the matrix outside the volume of material described by the plane of fibers and their thickness.

The fiber strength used in the model was computed from the observed $[0]_4$ behavior and the matrix strength computed from Neu's model. The predicted stress in the [0/90] composites was calculated as follows.

$$\sigma[0/90]_s = \frac{\sigma[0]_4}{2} + 2 * \sigma[90] \qquad (1)$$

where $\sigma[0]_4$ = measured stress in the $[0]_4$ composite specimen tests

$\sigma[90]$ = calculated stress in a 90° ply of the $[0/90]_s$ composite
$(= [d_{ply} - d_{fiber}] / d_{ply} * \sigma_{matrix})$

d_{ply} = thickness of the 90° ply (= 0.238 mm)

d_{fiber} = fiber diameter (= 0.140 mm)

σ_{matrix} = matrix stress computed from Bodner-Partom model.

Figure 7 compares the predictions and the measured values of stress in the $[0/90]_s$ tensile tests up to the maximum stress. The comparison shows very good agreement.

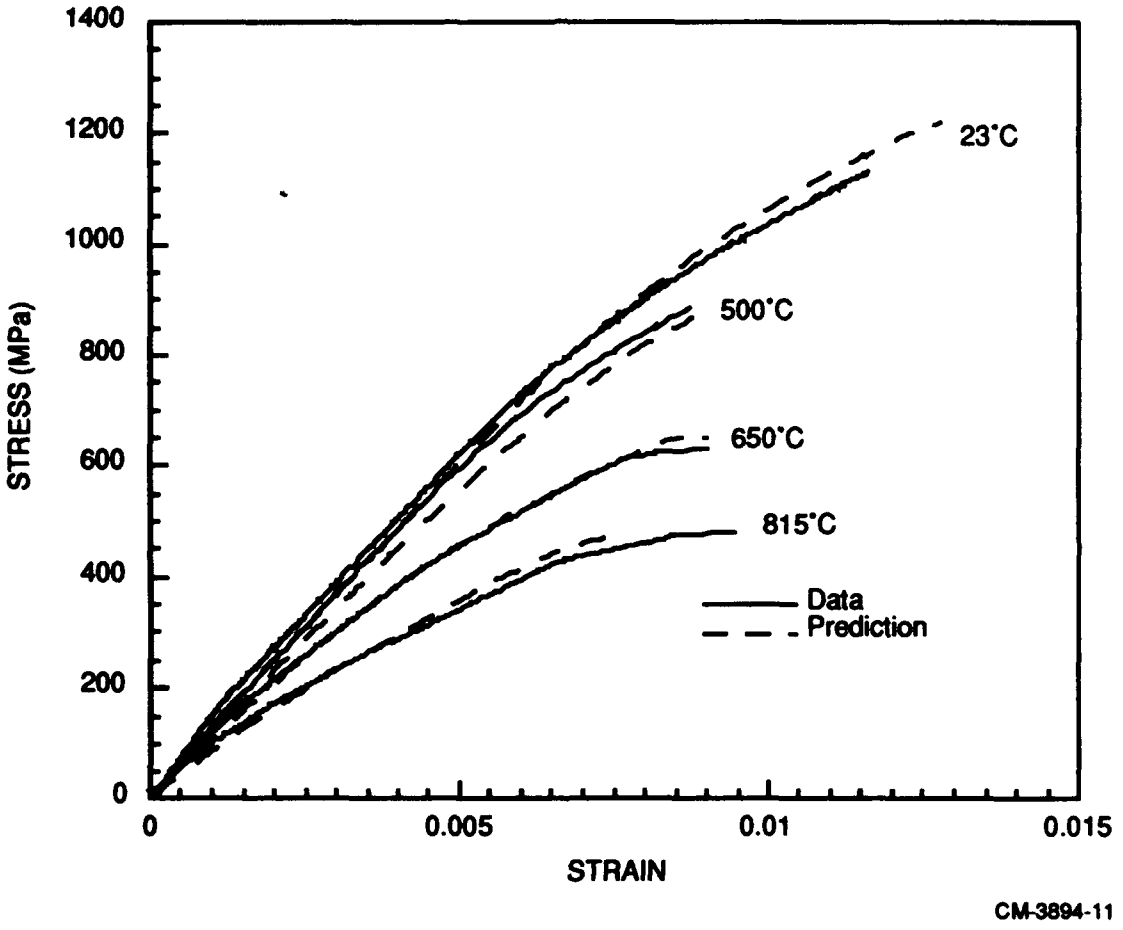

Figure 7. Comparison of measured and predicted stress-strain behavior for $[0/90]_s$ SCS6/Timetal 21-S composite based on $[0]_4$ data and Neu's model for Timetal 21-S.

DISCUSSION

The observation that matrix damage is preceded by fiber breakage is similar to the findings of others who have studied similar composites. Majumdar and Newaz[4] investigated the tensile properties of SCS6/Ti-15-3 composites with [0] and [90] fiber orientations. The Ti-15-3 alloy is about 25% weaker than Timetal 21-S but shares the characteristics of high ductility and weak bonding to SCS6 fibers. Majumdar and Newaz found that damage (i.e., cracking) in the [0] composite prior to the maximum load was generally confined to small cracks in the fiber/matrix interface that did not propagate into the fiber or the matrix. Also, Lerch[5] found extensive deformation but no cracks in the matrix of [0] specimens strained just short of the maximum load in a SCS6/Ti-15-3 composite. He reported the presence of matrix cracks only in composites with 30° plies.

Jeng, Yang, and Yang[6] and Yang and Jeng[7] classified the tensile behavior in a range of titanium alloy composites and found that the toughness of the matrix and the fiber strength/interface strength ratio were the most important variables. Although they did not report results on SCS6/Timetal 21-S, they did study titanium alloy composites with similar properties (i.e., composites with a high matrix toughness and a high fiber-to-interface strength ratio such as the SCS6/Ti-15-3 composite in the as-received condition). They state that in such cases tensile loading of [0] composites initiates cracking in the interface layer. These cracks are arrested by microyielding of the matrix but produce limited interfacial debonding between the matrix and the fiber on further loading. The remaining interfacial bonds are strong enough to transfer load back into the interfacial zone and continue to fracture the interface. Fracture of the composite is initiated by fiber fracture, which, in turn, occurs at randomly distributed weak spots in the fibers.

The present results fit the descriptive model of Jeng, Yang, and Yang in at least two respects: (1) damage (i.e., cracking) that occurs during loading is confined to a small region of the composite (the fiber/matrix interface), and (2) the failure of the fibers precedes matrix failure in the final stages of failure of the composite.

---

[4] B. S. Majumdar and G. M. Newaz, "Inelastic Deformation of Metal Matrix Composites: Plasticity and Damage Mechanisms," Phil. Mag. A, 66(2), 187-212 (1992).

[5] B. A. Lerch, "Matrix Plasticity in SiC/Ti-15-3 Composite," NASA Report No. NASA-TM-103760, July 1991.

[6] S. M. Jeng, J.-M. Yang, and C. J. Yang, "Fracture Mechanisms of Fiber-Reinforced Titanium Alloy Matrix Composites. Part II; Tensile Behavior," Materials Science and Engineering, A138, 169-180 (1991).

[7] J.-M. Yang and S. M. Jeng, "Deformation and Fracture of Ti-and Ti_3Al-Matrix Composites," Journal of Metals, pp. 52-57 (June 1992).

The observations that the final stages of composite fracture are initiated by the fibers and that the fibers carry most of the load have important implications for the analysis of the fracture surfaces. These observations suggest that the observable matrix fracture features reflect the failure processes occurring in the matrix after fiber failure. The loads that can be sustained by the matrix are small in comparison to those supported by the fibers, and the ductility of the matrix is significantly greater, so matrix fracture occurs after the maximum load of the composite is reached. Consequently, the matrix fracture surfaces that are observed reflect failure processes which occur in the final stage of composite failure in a tensile test. Detailed reconstruction of the fracture process—by fracture surface topography analysis (FRASTA), for example—will be strongly influenced by the matrix failure processes that occur immediately before final failure and only weakly influenced by the initiation and early stages of the failure process. The fact that no extraordinary stress-strain behavior was observed when a physically large inhomogeneity (the woof fiber) was present on the fracture surface also implies that the tensile behavior of the particular composite is not sensitive to the matrix behavior.

SUGGESTIONS FOR FUTURE RESEARCH

The weak correlation between tensile properties and fracture surface topography is not likely to persist in specimens subjected to other forms of loading. Thermomechanical loading is known to involve an interplay between matrix dominated behavior and fiber dominated behavior. For example, Mall et al.[8] found that out-of-phase thermal and mechanical cyclic conditions produced failures that were matrix dominated, whereas fiber dominated behavior was observed under in-phase or isothermal conditions. Different heat treatment conditions can also profoundly affect the role of the matrix, interface, and fiber. Yang and Jeng[7], for example, found that interface conditions and fiber strength could be altered by heat treatment of the composite so that matrix dominated or fiber dominated failures would result.

To fully exploit the capabilities of quantitative fracture surface analysis in understanding the role of the matrix, fiber, and interface in determining the mechanical properties of SCS6/Timetal 21-S composites, we recommend that fracture surface analyses focus on fatigue loading, material condition variables, and, perhaps, environmental variables. An understanding of conditions where matrix failure plays a dominant or at least a significant role in determining composite behavior will

---

[8] S. Mall, D. G. Hanson, T. Nicholas, and S. M. Russ, "Thermomechanical Fatigue Behavior of a Cross-Ply SCS-6/β21-S Metal Matrix Composite," in *Constitutive Behavior of High Temperature Composites*, MD-Vol. 40, B. S. Majumdar, G. M. Newaz, and S. Mall, Eds. (American Society of Mechanical Engineers, New York, 1992), pp. 91-106.

enable conclusions to be drawn about the initiation and development of failures in SCS6/Timetal 21-S composites and hence provide the basis for tailoring these materials to specific aerospace applications.

SUMMARY

The following inferences can be drawn as a result of the accurate predictions of the $[0/90]_s$ stress-strain curves and the results of analyses of the $[0]_4$ composite:

- Failure of the matrix occurs after the maximum load is reached and after some or all of the 0° fibers have failed, as implied by the accurate prediction of the stress-strain curve up to the maximum stress by a model that assumes no damage (i.e., cracking) occurred in the matrix.

- Only part of the matrix phase of the 90° plies in a $[0/90]_s$ composite contributes to the tensile strength. The interface strength between the fibers and the matrix is negligible and does not contribute significantly to the strength of the composite. This finding is consistent with the findings of other studies[1,2] of the same composite.

- The topography of the matrix fracture surface is a strong function of processes that occur during the rapid reduction in load after the maximum load. Events in this regime have little, if any, effect on the stress-strain response of the composite.

- The presence of the woof fiber on the fracture surface of the 23°C test of the $[0]_4$ composite appears to have little or no effect on the tensile behavior of that specimen. This conclusion is based on the accurate prediction of the $[0/90]_s$ composite behavior on the basis of results from the $[0]_4$ composite without any allowance for the presence of the woof fiber.

Future fracture surface analyses of the SCS6/Timetal 21-S composites will focus on the effects of fatigue loading, material condition variables, and, perhaps, environmental variables.